Accurate buoyancy and drag force models to predict particle segregation in vibrofluidized beds

Mehrdad Kiani Oshtorjani,[1,*] Liu Meng,[2,*] and Christoph R. Müller[2]

[1]*Laboratory of Environmental Hydraulics, Department of Mechanical Engineering, École Polytechnique Fédérale de Lausanne, Écublens, 1015 Lausanne, Switzerland*

[2]*Laboratory of Energy Science and Engineering, Department of Mechanical and Process Engineering, ETH Zurich, Leonhardstrasse 21, 8092 Zurich, Switzerland*

(Received 28 February 2021; accepted 20 May 2021; published 14 June 2021)

The segregation of large intruders in an agitated granular system is of high practical relevance, yet the accurate modeling of the segregation (lift) force is challenging as a general formulation of a granular equivalent of a buoyancy force remains elusive. Here, we critically assess the validity of a granular buoyancy model using a generalization of the Archimedean formulation that has been proposed very recently for chute flows. The first model system studied is a convection-free vibrated system, allowing us to calculate the buoyancy force through three different approaches, i.e., a generalization of the Archimedean formulation, the spring force of a virtual spring, and through the granular pressure field. The buoyancy forces obtained through these three approaches agree very well, providing strong evidence for the validity of the generalization of the Archimedean formulation of the buoyancy force which only requires an expression for the solid fraction of the intruder, hence allowing for a computationally less demanding calculation of the buoyancy force as coarse graining is avoided. In a second step, convection is introduced as a further complication to the granular system. In such a system, the lift force is composed of granular buoyancy and a drag force. Using a drag model for the slow-velocity regime, the lift force, directly measured through a virtual spring, can be predicted accurately by adding a granular drag force to the generalization of the Archimedean formulation of the granular buoyancy. The developed lift force model allows us to rationalize the dependence of the lift force on the density of the bed particles and the intruder diameter, the independence of the lift force on the intruder diameter, and the independence of the lift force on the intruder density and the vibration strength (once a critical value is exceeded).

DOI: 10.1103/PhysRevE.103.062903

I. INTRODUCTION

Segregation is commonly observed in granular materials that contain a mixture of particles that differ in size [1–4], density [5,6], shape [7] or mechanical properties (friction, elasticity) [8,9]. A fundamental understanding of the physics behind segregation in granular materials is not only a scientific curiosity [10–12], but also of high relevance for practice. In practical applications such as the mixing of pharmaceutical ingredients [13], the filling (and discharge) of hoppers [14], or the transport of granular media through agitation (e.g., vibration) from one processing unit to the other [15,16], size - and density-induced segregation is unavoidable and has to be controlled or at least minimized when designing unit operations or granular conveyer systems. In most industrial applications such as the food or pharmaceutical industries a well-mixed state is desired and indeed critical to ensure the desired product specification, hence an in depth understanding of the parameters controlling segregation is critical. Besides the industrial relevance of segregation, it also prevails in dynamic natural phenomena such as debris flow [17]. A well-studied segregation phenomenon is the so called "Brazil nut phenomenon" (BNP) [18], which describes the upward motion of an intruder in a vibrating granular bed, where the intruder diameter is larger than the diameter of the bed particles.

A. Qualitative models

Depending on the vibration strength, the BNP can be rationalized by one of the following two models: The first model is valid for low vibration strengths (typically low or even irregular vibration frequency); the upward migration of the intruder is explained by the arch (or vault) effect, whereby upon an upward movement of the intruder, voids are formed at the bottom part of the intruder. A new, higher, intruder position in the bed is stable if the large intruder is supported by at least two particle contacts below its center of gravity (two-dimensional case). Small bed particles are able to easily fill the voids below the intruder leading to a continuous upward motion of the intruder through a series of stable intruder "jumps." This explanation has been termed also the percolation model [1,18–21]. In such a segregation regime, a critical minimal size of an intruder compared to the bed particle size is required to trigger segregation [19–21] and the rise velocity of the intruder increases with increasing intruder size [19]. According to the second model, which is valid under conditions of high vibration strength (typically a high vibration frequency), a convection cell establishes in the vibrating bed. This convection cell carries the intruder upward in the center of the bed, leading to a rise velocity of the intruder that is

[*]These authors contributed equally to this work.

independent of the ratio of the intruder size to bed particle size [22]. The region of downward particle motion at the walls is thin, making it impossible for the large intruder to be convected downward once it has reached the top surface of the bed [19,23]. Depending on the type and strength of agitation of a granular bed, the intruder size [1,19,24] and/or density [25–27] is known to affect the tendency for segregation. In general, bigger and lighter intruders segregate more favorably.

B. Quantitative models

In recent years, attempts have been made to develop not only qualitative, but also quantitative segregation models, which requires a hydrodynamic description of a segregating granular bed. So far, no model has been found which describes a segregation force on an intruder that is generally applicable. Instead, separate models have been developed which are only applicable to either dilute [28,29] or dense granular systems [4,7,30]. Additionally, among the models for dense systems one finds different models for either sheared systems, i.e., systems with convective particle motion, or vibrated systems with no inherent convective motion.

1. Buoyancy force in dilute vibrated systems

In this context, Shishodia and Wassgren [27] modeled the segregation of intruders in a two-dimensional (2D) vibrofluidized bed using the discrete element method (DEM), i.e., a Lagrangian modeling approach that is related to molecular dynamics simulations. They considered a shallow bed, i.e., the ratio of the bed height to width was <1, that contained frictionless particles. A consequence of this dilute vibrated bed was that the vertical granular pressure gradient was constant only over a very small height, with increasing and decreasing pressure gradients with a vertical position below and above the center of the bed, respectively. Shishodia and Wassgren [27] observed that upon vibration the intruder reached an equilibrium position within the bed. At the equilibrium position, the downward directed gravitational force is balanced by a net lift force due to particle-intruder contacts. The vertical position of the equilibrium position of the intruder was found to increase with increasing vibration strength, decreasing density ratio of the intruder to the bed particles, and increasing coefficient of restitution. Subsequently, Shishodia and Wassgren [27] developed a hydrodynamic model of the granular system to predict the equilibrium position of the intruder, whereby a buoyancy force F_b, which balances the intruder weight, arises from the net pressure in the system:

$$F_b = \oint p \cdot \mathbf{n} d\mathbf{s}. \tag{1}$$

In a 2D granular system, the (granular) pressure is $P = 1/2(\tau_{s,xx} + \tau_{s,yy} + \tau_{c,xx} + \tau_{c,yy})$, where $\tau_{s,xx}$ and $\tau_{s,yy}$ are the streaming normal stresses and $\tau_{c,xx}$ and $\tau_{c,yy}$ are the collisional normal stresses [27,31]. In two dimensions, the streaming normal stresses are given by $\tau_{s,xx} = \rho_p \phi \langle u'^2 \rangle$ and $\tau_{s,yy} = \rho_p \phi \langle v'^2 \rangle$, where ρ_p is the particle density, ϕ is the mean solid fraction, and u' and v' are the velocity fluctuations in the horizontal and vertical directions, respectively. Here, $\langle\ \rangle$ denotes a temporal average. The collisional normal stresses are given by $\tau_{c,xx} = \frac{\Sigma r_p \mathbf{J}\cdot\mathbf{e}_x}{W \Delta y_{\text{bin}} \Delta t}$ and $\tau_{c,yy} = \frac{\Sigma r_p \mathbf{J}\cdot\mathbf{e}_y}{W \Delta y_{\text{bin}} \Delta t}$ [27], where r_p is the radius of the bed particles, $\mathbf{J}$ is the momentum exchange during a collision, W and Δy_{bin} are the width and height of the sampling bin, respectively, and $\mathbf{e_x}$ and $\mathbf{e_y}$ are the unit vectors along the x and y directions. The summation is performed over all collisions occurring within time Δt in a given bin. Shishodia and Wassgren [27] postulated that at equilibrium, the pressure force acting on the intruder (i.e., buoyancy) balances the particle weight, yielding (in a 2D system)

$$\frac{dp}{dy} = \frac{-m_I \mathbf{g}}{\pi d_I^2} = -\rho_I \mathbf{g}, \tag{2}$$

i.e., an intruder that is larger than the bulk particles will rise up to the position where the pressure gradient equals $-m_I g/\pi d_I^2$,, where m_I and d_I are the mass and diameter of the intruder, respectively. This model relies on the assumption that the presence of an intruder does not affect the pressure field of the system that is established without the presence of an intruder. Using Eq. (2) in combination with a given pressure profile in the granular bed, the equilibrium position of an intruder can be calculated. When the mass of the intruder becomes too large (to be supported by the pressure gradient), the intruder sinks to the base plate and oscillates synchronously with the base plate. However, Shishodia and Wassgren [27] noted that the findings of their model might not be readily extrapolated to deep granular beds due to a large number of nonbinary contacts, the possible occurrence of convective patterns, and the effects of an interstitial fluid.

2. Lift force in dense sheared systems

More recently, also the hydrodynamic modeling of segregation in dense shear flows has attracted appreciable interest [30,32–34]. For example, Guillard *et al.* [30] proposed scaling laws for the segregation force acting on single intruder in 2D, dense shear flows. In their shear flow simulations, the particles were modeled by DEM with the gravitational vector varying from vertical to horizontal directions. The segregation (or lift) force was measured via a virtual spring and was found to be proportional to the pressure gradient and shear stress gradient (i.e., buoyancylike forces), viz.,

$$F_{\text{lift}} = -\frac{\pi d_I^2}{4}\left(F\frac{\partial p}{\partial y} + G\frac{\partial |\tau|}{\partial y}\right), \tag{3}$$

where F and G are empirically derived functions of the friction coefficient $\mu = |\tau|/p$ and size ratio d_I/d_p. Interestingly the segregation force was found to have a maximum at $d_I/d_p \sim 2$ and switching off gravity resulted in a zero segregation force owing to a uniform pressure distribution in the bed.

van der Vaart *et al.* [34] followed up on the work of Guillard *et al.* [30] aiming to shed more light on the origin of the segregation (lift) force in 3D monodisperse, dense shear flows. Unlike Guillard *et al.* [30], van der Vaart *et al.* [34] modeled the segregation force acting on the intruder F_{lift} as the sum of a Saffman-like lift force and a generalized buoyancy force that depends on the ratio of the diameter of the intruder to the diameter of the bed particles, i.e., $F_{\text{lift}} = F_{\text{saff}} + F_b$, where F_{lift} is the total lift (segregation) force, F_b is the buoyancy, and F_{saff}

is the Saffman force. van der Vaart *et al.* [34] argued that the granular buoyancy force arises from the hydrostatic pressure acting on the Voronoi surface of the intruder, yielding a more generalized expression of the buoyancy force [34], viz.,

$$F_b = \oint p\mathbf{n}\cdot d\tilde{\mathbf{S}}_I = \phi\rho_p g\int_{\tilde{V}_I} dV$$
$$= \phi\rho_p g\tilde{V}_I = \frac{\phi}{\phi_I}\rho_p g V_I, \tag{4}$$

where $\tilde{S}_I$ is the surface of the Voronoi volume of the intruder, $\tilde{V}_I$ is the Voronoi volume of the intruder, P is the hydrostatic pressure, and $\mathbf{n}$ is the outward-directed normal vector to $\tilde{S}_I$. The Voronoi volume of a particle in a granular system is the volume of a cell that contains all of the space that is closer to the particle considered than any other particle. Equation (4) differs from the classic Archimedean formulation of a buoyancy force in a granular media, i.e., $F_b = \phi\rho_p g V_I$, as it is a function of d_I/d_p (with $F_b = m_I g = F_g$ for $d_I/d_p = 1$). Using DEM simulations, the empirical equation $\phi_I = (\phi - 1)(d_I/d_p)^c + 1$ ($c = -1.2$ and $\phi = 0.577$) was obtained. Subtracting the granular buoyancy force from the contact force F_c a granular Saffman-type lift (segregation) force was obtained and expressed as $F_{\text{saff}} = -\lambda_x\eta b I_\theta \mu^{-0.5} d_I^2 d_p^{-1}\text{sng}(\dot{\gamma})$, where $\lambda_x = \langle v_{Ix}(t) - v_x(z_I, t)\rangle$ is the velocity lag of the intruder with respect to the bulk downstream flow, $\eta = |\tau|/\dot{\gamma}$ is the granular viscosity, $I_\theta = \dot{\gamma}d/(P/\rho)^{0.5}$ is the inertial number, $\mu = |\tau|/P$ is the bulk friction coefficient, $\dot{\gamma}$ is the local shear rate, and a is a fitting parameter.

3. Buoyancy in dense convection-free systems

In the systems described above (Sec. II) a shear flow has been present. Hence, granular drag and/or forces arising from velocity gradients might affect segregation making in turn the elucidation of the contribution of the buoyancy force on segregation challenging if not even impossible. An ideal system to study segregation would be free of a convective flow pattern. To avoid convection in a vibrated bed, Huerta *et al.* [35] proposed an experimental setup to vibrate the lateral walls of the bed such that adjacent walls move out of phase ($\varphi_2 - \varphi_1 = \pi$), ensuring an almost constant bed volume. Indeed, Huerta *et al.* [35] could not observe any convective patterns, which was probed by placing tracer particles. Subsequently, Huerta *et al.* [35] measured the lift force (which is equal to the buoyancy force in a convection or velocity-free system) acting on the intruder using a dynamometer that was connected with a wire to the intruder. Key observations of the experimental work of Huerta *et al.* [35] were (i) the buoyancy force becomes independent of Γ for $\Gamma \geqslant \Gamma_{cr} = 5$, and (ii) the buoyancy force follows Archimedes' principle, i.e., buoyancy is proportional to the volume displaced. However, fitting the experimentally determined buoyancy force as a function of the intruder volume V_I gives a positive intercept for $V_I = 0$, which might suggest that a classic Archimedean formulation of the buoyancy force underestimates the buoyancy force as V_I approaches small values. This observation was explained by Huerta *et al.* [35] by the argument that when the intruder size approaches the size of the bed particle, the intruder becomes indistinguishable from the bed material and they suggested that buoyancy only occurs for intruders that are "considerably larger than the volume of the beads."

4. Drag force in convective systems

However, in most of the naturally and industrially prevalent granular systems, convection is inherent. Hence, when studying the segregation dynamics of intruders in such systems, the drag force acting in the opposite direction to the (relative) intruder motion has to be considered. Generally, two different drag regimes have been considered, viz., a slow- and a rapid-velocity regime [36,37]. The motion of an intruder in dense vibrating beds, i.e., the system considered in our work, will typically fall into the slow-velocity regime in which the drag force is independent of the relative intruder velocity. Albert *et al.* give a commonly used drag force correlation for a discrete object with a circular cross sectional area in the slow flow regime [36,38] as

$$F_d = \eta g\rho_p(y_h - y)d_I^2, \tag{5}$$

where ρ_p is the density of the bed particles, d_I is the diameter of the intruder, y_h is the filling height of the bed, y is the intruder position along the bed height, and $\eta = B\sqrt{32\pi^2/27e^2}$, where e is the coefficient of restitution and B is a constant depending on the surface properties, morphology, and packing of the grains. The independence of the drag force on the intruder velocity in the slow-velocity regime has been confirmed by Reddy *et al.* [39].

5. A general segregation force

Here we propose a segregation model, which is generally applicable to dense systems, with and without convective motion. To this end, a model system is created where convection can be turned on or off by switching friction between particles and walls on or off. Switching wall friction on introduces an upward convection in the center of the bed which in turn leads to a drag force on the intruder. By subtracting the buoyancy, which is determined by the generalized buoyancy model, from the lift force, we could obtain the drag force, i.e., $F_d = F_{\text{lift}} - F_{\text{b}}$, which suggests that the value of F_d depends on the chosen buoyancy model. By confirming whether the drag force agrees with the granular drag model, Eq. (5), we could further verify and extend the applicability of the generalized Archimedean principle in the system under consideration.

The first objective of our work is to probe numerically the validity of a generalized Archimedean formulation, Eq. (4), to describe a granular buoyancy force. Eq. (4) has been proposed for chute flows and takes into account the solid fraction around an intruder. To this end we use a model system, i.e., a vibrating bed that is free from convection (zero wall friction). The vibrating bed is vibrated horizontally and the validity of Eq. (4) is assessed by measuring the magnitude of the buoyance force through a virtual spring force F_s via $F_b = F_s + mg$ and through its definition by integration of the stress tensor on the intruder surface [Eq. (1)].

We subsequently expand our study to a system that contains convection (by imposing friction to the side walls) which inevitably introduces also a drag force that acts onto the intruder. The drag force is determined by subtracting the

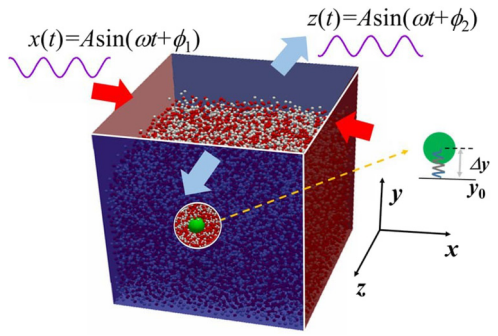

FIG. 1. Illustration of the simulated granular system. An intruder is immersed inside the granular bed and connected to a virtual spring. The lift force is determined via the measured spring force, i.e., $\mathbf{F}_{\text{lift}} = -(\mathbf{F}_s + \mathbf{F}_g)$, where the spring force is calculated using Hooke's law, $F_s = k\Delta y \mathbf{e}_y$, where k is the spring stiffness of the virtual spring and Δy is the vertical displacement of the intruder compared to its initial position. The sidewalls are vibrated such that the two walls (red wall) opposite each other follow the displacement $x(t) = \pm A_0 \sin(\omega t + \phi_1)$ with A_0 being the amplitude and $f = \omega_0/(2\pi)$ the frequency of the excitation. The vibration of the other two side walls (blue wall) is given by $z(t) = \pm A_0 \sin(\omega t + \phi_2)$, hence adjacent walls move out of phase by $\phi_2 - \phi_1 = \pi$.

buoyancy force [Eq. (4)], from the total lift force, i.e., $F_d = F_{\text{lift}} - F_{\text{b}}$ and through a granular drag force formulation.

Using a granular drag force formulation, we are able to correctly predict the segregation (lift) acting on an intruder in a granular system and to correctly predict the dependence of the lift force on a variety of system parameters, hence providing a general modeling framework to predict the segregation and buoyancy forces on granular intruders in dense granular systems with and without convection, i.e., sheared and vibrated.

II. METHOD

In this work, the system under investigation is a rectangular bed containing 27 000 particles [Fig. 1]. To allow a comparison with the experimental work of Huerta *et al.* [35] the following particle mixture is used: a 50:50, bidispersed mixture of glass beads of radii 1.5 and 2.0 mm (density of 2240 kg/m^3). The length, width, and filling height of the container are $x = 0.107$ m, $z = 0.107$ m, and $y = 0.095$ m, respectively. The lateral walls of the container are excited sinusoidally in the xz plane. Two walls opposite each other vibrate by imposing the displacement $x(t) = \pm A_0 \sin(\omega t + \phi_1)$ with A_0 being the amplitude and $f = \omega_0/(2\pi)$ the frequency of the excitation. The vibration of the other two side walls is given by $z(t) = \pm A_0 \sin(\omega t + \phi_2)$, hence adjacent walls move out of phase by $\phi_2 - \phi_1 = \pi$. Such a vibration leads to an almost constant square area (+/−0.07%) with time, avoiding arguably the formation of convection patterns. Inside the bed, an intruder is placed at the coordinates (0 m, 0.05 m, 0 m) and the vibration is initiated at $t = 0$ s. The intruder diameter was varied from $1.67\bar{d}_p$ to $12\bar{d}_p$ in the simulations, where $\bar{d}_p$ is 3.5 mm, which is the average bed particle diameter of the system.

TABLE I. Material properties used.

Parameters	Value
Poisson's ratio of the particles	0.45
Restitution coefficient of particle-wall contact	0.6
Restitution coefficient of particle-particle contact	0.6
Shear modulus of wall-particle contact	5.0×10^6 Pa
Shear modulus of particle-particle contact	5.0×10^6 Pa
Time step	10^{-5} s
Total simulation time	200 s
Friction coefficient for particle-wall contact	0.5
Friction coefficient for particle-particle contact	0.5
Normal contact stiffness	4.18×10^6 N/m

The vibration strength, $\Gamma = A_0\omega_0^2/g$, applied in this work ranged from $\Gamma = 2.51$–60 (varied through changes in the frequency while keeping the amplitude fixed at $A_0 = 1$ mm). The interactions between the particles were modeled via a discrete element method (DEM) [40] using the open source LIGGGHTS package [41]. A spring-dashpot model describes the collisional forces (normal F_{nij} and tangential contact force F_{tij}):

$$\mathbf{F}_{nij} = \sqrt{\delta_{nij}R^*}(k_n\delta_{nij}\mathbf{n}_n - \eta_n\mathbf{v}_{nij}), \tag{6}$$

$$\mathbf{F}_{tij} = \sqrt{\delta_{tij}R^*}(-k_t u_{ij}\mathbf{n}_t - \eta_t\mathbf{v}_{tij}), \tag{7}$$

where k_n and k_t are the spring constants in the normal and tangential direction (given by $k_n = 4/3E^*$ and $k_t = 8G^*$, with $E^* = ([1-v_i^2]/E_i + [1-v_j^2]/E_j)^{-1}$ and $G^* = ([2-v_i^2]/G_i + [2-v_j^2]/G_j)^{-1}$ where $E_{i,j}$, v_{ij}, and G_{ij} are the particle's Young's modulus, the Poisson ratio, and the shear modulus, respectively). Further, η_n and η_t are the damping coefficients in the normal $\mathbf{n}_n$ and tangential $\mathbf{n}_t$ directions, respectively. The overlap between two particles in the normal direction is $\delta_{nij} = |\mathbf{u}_i - \mathbf{u}_j|\Delta t$, where $\mathbf{u}_i$ and $\mathbf{u}_j$ are the velocities of the ith and jth particle at t_0 and Δt is the time interval. The tangential displacement of a contact is calculated as $u_{tij} = (\mathbf{u}_{ik} - \mathbf{u}_{jk})\mathbf{n}_n\Delta t - (\boldsymbol{\omega}_{j(k+1)}\mathbf{n}_{k+2} - \boldsymbol{\omega}_{j(k+2)}\mathbf{n}_{k+1})r_i\Delta t - (\boldsymbol{\omega}_{i(k+1)}\mathbf{n}_{k+2} - \boldsymbol{\omega}_{i(k+2)}\mathbf{n}_{k+1})r_j\Delta t$, where k rotates from x to z, r_i and r_j are the radius of the ith particle and the jth particle respectively, and ω is the angular velocity. The tangential contact force is limited by Coulomb's law, i.e., $|F_{tij}| \leqslant \mu|F_{ni,j}|$. A summary of the values of the modelling parameters used in this work is given in Table I.

To determine the segregation force acting on the intruder, a virtual spring is used [30]. The virtual spring connects the center of the intruder to its initial position (0 m, 0.05 m, 0 m) (Fig. 1). In the system modeled (convection free), three forces act on the intruder: (i) gravitation F_g, (ii) the force exerted by the virtual spring F_s, and (iii) the lift force arising from the contacts between the bed particles and the intruder (the lift force is commonly also referred to as the segregation force) [30,34]. Hence, at equilibrium the lift force acting on the intruder is balanced by

$$\mathbf{F}_{\text{lift}} = \mathbf{F}_c = -(\mathbf{F}_g + \mathbf{F}_s), \tag{8}$$

where $\mathbf{F}_c$ is (the sum of) the contact forces acting between the intruder and the surrounding bed particles, $\mathbf{F}_s =$

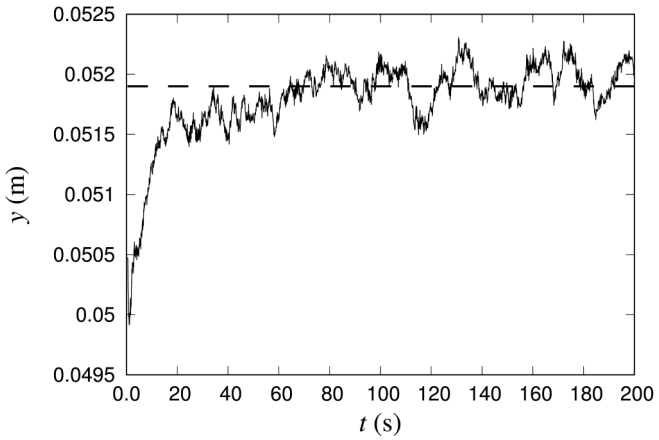

FIG. 2. Vertical position of an intruder tracked over 200 s. The dashed horizontal line corresponds to the equilibrium position around which the intruder oscillates.

$-k(y-y_0)\mathbf{e}_y$, with k being the stiffness of the virtual spring, y is the average vertical position of the intruder for a given setting, and y_0 is the initial position of the intruder that is fixed to $y_0 = 0.05$ m. As an example, Fig. 2 plots the instantaneous vertical position of an intruder as a function of time over 200 s.

From Fig. 2 we can observe that the intruder rises quickly and reaches an equilibrium position, around which it oscillates after ∼20 s. The values of the intruder position reported in the following are the values obtained in this equilibrium state (with simulations typically being performed over 200 s). To assess whether the magnitude of the spring stiffness of the virtual spring affects the numerical results, simulations were repeated for varying values of k. As shown in Fig. 3 the lift force is independent of the spring stiffness k for $5\,\mathrm{N/m} < k < 200\,\mathrm{N/m}$, in agreement with a previous report [30]. The inset in Fig. 3 plots $\Delta y = y - y_0$ of the intruder, normalized by the intruder diameter, as a function of the normalized spring stiffness of the virtual spring. The slope of this line, multiplied by the diameter of the intruder d_I and the normal stiffness

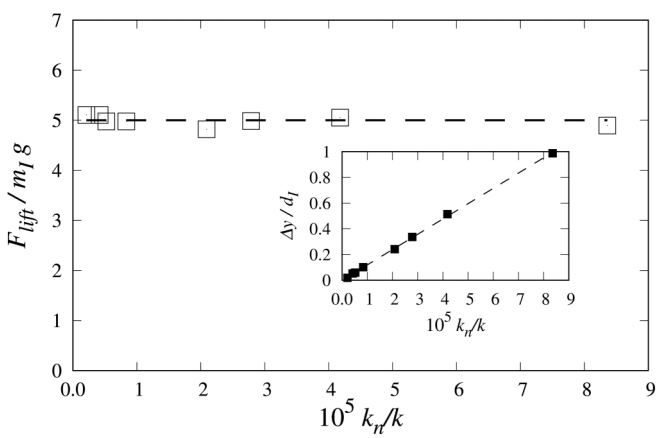

FIG. 3. Normalized segregation (lift) force as a function of the spring stiffness k normalized by the stiffness of the interparticle force, i.e., $k_n = 4.18 \times 10^6$ N/m. Inset: $\Delta y = y - y_0$ of the intruder as a function of the normal spring stiffness of the virtual spring.

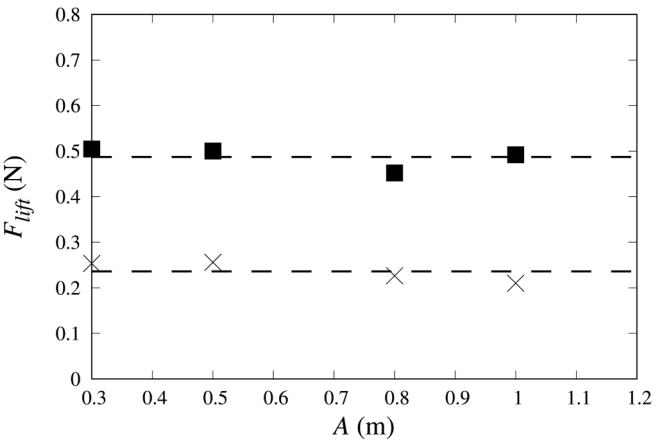

FIG. 4. Lift force versus vibrational amplitude A, × : $\Gamma = 8.0$, $d_I/d_p = 5$ and ■ : $\Gamma = 20.0$, $d_I/d_p = 7$.

of the interparticle collisions k_n, is equal to the spring force. Owing to the very high linearity, the lift force acting on the intruder can be determined via Eq. (8). In this work a constant spring stiffness of $k = 80\,\mathrm{N/m}$ was used for the virtual spring.

We further assessed the sensitivity of the determined segregation force to the amplitude A and the angular frequency ω of the vibration. Figure 4 confirms that the lift force is not sensitive to the amplitude and angular frequency of the vibration for a given vibrational strength Γ.

III. RESULTS

Prior to assessing the validity of the different granular buoyancy models, we performed a sensitivity analysis of the dependence of the lift force on the dimensionless vibration strength Γ, as a minimal value of Γ is required to fluidize the system [5,35]. Figure 5 plots the lift force [Eq. (8)] as a function of Γ. Similar to the experimental observation of Heuta *et al.* [35], we also observe that the lift force reaches asymptotic values for $\Gamma > 6$ (inset of Fig. 5). The reason for a

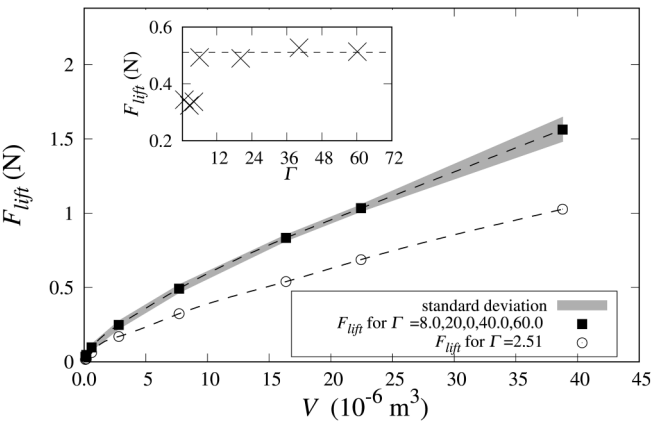

FIG. 5. Lift force as a function of the volume of the intruder for five different vibration strengths grouped as $\Gamma = 2.51 < \Gamma_{cr}$ and $\Gamma = 8.0, 20.0, 40.0, 60.0 > \Gamma_{cr}$ where $\Gamma_{cr} = 6$ is the critical vibration strength. Inset: Lift force as a function of vibration strength (dI/dp) to determine Γ_{cr}.

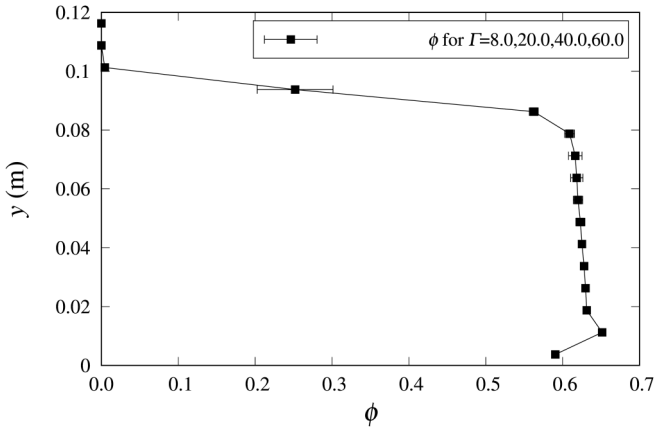

FIG. 6. Profile of the solid volume fraction ϕ in the bed as a function of the y direction for $8 < \Gamma < 60$.

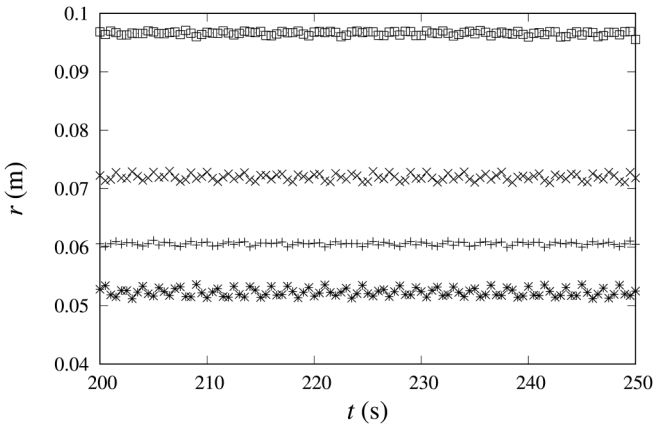

FIG. 7. Temporal evolution of position $r = (x^2 + y^2 + z^2)^{0.5}$ of randomly selected particles in the bed, when the friction coefficient for wall-particle collisions is set to zero ($\Gamma = 8.0$).

decreasing lift force for $\Gamma < \Gamma_{cr}$ is that under these conditions only the regions close to the walls are fluidized whereas the center of the bed is only poorly fluidized, leading in turn to reduced segregation dynamics. Indeed, when Huerta *et al.* [35] inserted two small intruders into a bed that was kept at $\Gamma < \Gamma_{cr}$ (one intruder was placed close to the walls and the other one in the center of the bed) the intruder closer to the wall segregated faster to the top surface. Overall, the value of $\Gamma_{cr} \sim 6$ as determined in our simulations is close to the experimental value of $\Gamma_{cr} = 5$ of Huerta *et al.* [35]. Once the bed is completely fluidized, a further increase in Γ does not have any appreciable effect on the lift force. Indeed, Fig. 5 confirms that the magnitude of the lift force does not vary with Γ for $8 < \Gamma < 60$. In addition to the lift force, also the solid fraction in the bed ($\phi = 0.62$) is largely unaffected by Γ when $\Gamma > \Gamma_{\rm cr}$ (Fig. 6). Overall the solid fraction is very homogeneous along the height of the bed, except at the bottom, i.e., $y < 0.02$ m and close to the surface, i.e., $y > 0.075$ m of the bed where smaller values of ϕ are observed.

To probe the validity of the generalized Archimedean formulation of the granular buoyancy force, Eq. (4), a system free of convective patterns is critical to exclude the presence of any additional forces, e.g., Saffman-type or drag forces. By setting the friction coefficient for particle-wall contacts to zero, we were able to establish an agitated (fluidized) system without any convection pattern being present. Tracing some randomly selected particles in the bed for 100 s, we could confirm the absence of any coherent motion in the bed (Fig. 7). In the absence of a convective pattern, the lift force $F_{\rm lift}$ is equal to the buoyancy force F_b and can be calculated by subtracting the gravitational force of the intruder from the measured spring force [Eq. (8)]. The buoyancy force calculated through Eq. (8) can then be compared to the prediction of F_b via a generalized Archimedean formulation [Eq. (4)] using the Voronoi volume of the intruder $\tilde{V}_I$. The Voronoi volume of the intruder is illustrated in Fig. 8. The solid fraction of the intruder ϕ_I is determined as the ratio of its (particle-based) volume ($V_I = 1/6\pi d_I^3$) and its Voronoi volume. Figure 8 shows that when the intruder size approaches the size of the bed particles, ϕ_I approaches the bulk solid fraction of the bed, i.e., $\phi_I = 0.62$. On the other hand, for very large intruder sizes, ϕ_I approaches asymptotically to 1. The numerically derived values of ϕ_I can be fitted well by the following functional form: $\phi_I = (\phi - 1)(d_I/d_p)^c + 1$ with $c = -1.2$. Our value of c is slightly different than the value reported by van der Vaart *et al.* [34] ($c = -1.35$) who studied, however, sheared systems containing monodispersed particles.

Figure 9 plots a comparison of the buoyancy force determined through the virtual spring [Eq. (8)] with the generalized Archimedean formulation of a granular buoyancy force [Eq. (4)]. The prediction obtained through the generalized Archimedean principle [Eq. (4)] and the buoyancy force obtained directly from the DEM simulations through the virtual spring force [Eq. (8)] agree very well, while some deviations are observed for high ratios of the intruder diameter to the diameter of the bed particles ($d_I/d_p = 7$). This deviation is most likely due to the fact that for such high aspect ratios the upper part of the intruder ($y_I \cong 0.076$ m) is very close to the bed surface, i.e., an area where the solid fraction of the bed is reduced appreciably (see Fig. 6). The lower solid fraction near the bed surface reduces the magnitude of the total contact

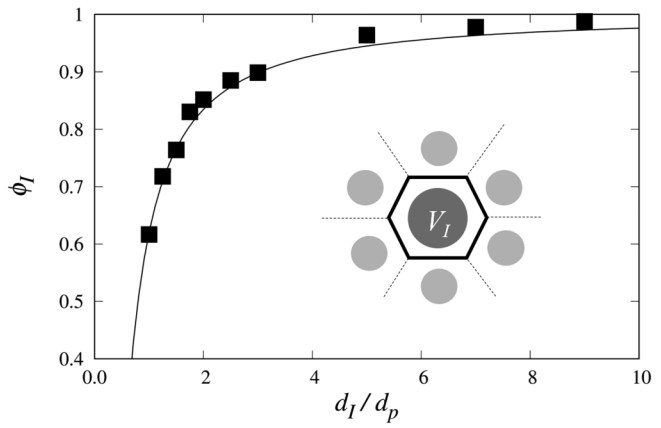

FIG. 8. Solid volume fraction of the intruder ϕ_I as a function of d_I/d_p for $\Gamma = 8$, $k = 80$ N/m. The closed area around the intruder which is bounded by a bold solid line gives the Voronoi volume $\tilde{V}_I$ of the intruder.

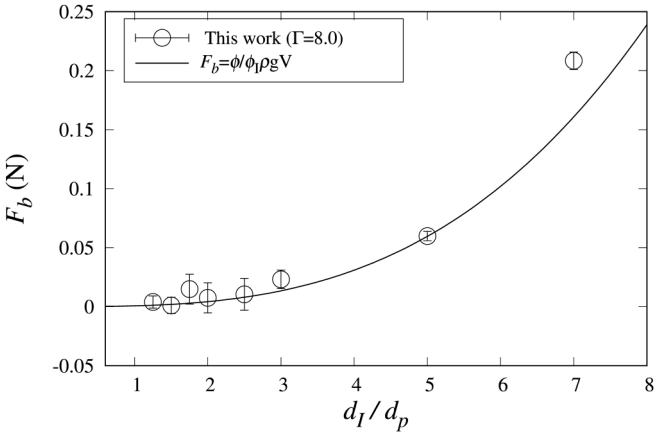

FIG. 9. Comparison of the generalized Archimedean formulation of the granular buoyancy force [Eq. (4)] with the buoyancy force determined by the virtual spring force $\mathbf{F}_{\text{lift}} = -(\mathbf{F}_s + m_I\mathbf{g})$ in a vibrated bed with $\Gamma = 8.0$.

forces on the upper part of the intruder (downward directed) hence increasing artificially the buoyancy of the intruder.

Besides Eqs. (4) and (8) the buoyancy force can be determined also through its formal definition, i.e., by integrating the pressure field over the (Voronoi) surface of the intruder [27,30,34], i.e.,

$$F_b = \oint p\mathbf{n}\cdot\mathbf{e}_y d\tilde{S}, \tag{9}$$

where $\tilde{S}_I$ is the Voronoi surface of the intruder. The coarse-graining (CG) method is used to calculate the (granular) pressure in the vibrated bed [42–44]. Here, we consider N particles in a control volume (also termed coarse-graining volume) whereby the center of mass of particle α is at $\mathbf{r}_\alpha$ (particle α moves with speed u_α). In a granular media the stress tensor $\sigma_{ij}(\mathbf{r},t)$ is composed of the so-called kinetic stress $\sigma^k_{ij}(\mathbf{r},t)$ and the collisional stress $\sigma^c_{ij}(\mathbf{r},t)$, viz., $\sigma_{ij}(\mathbf{r},t) = \sigma^k_{ij}(\mathbf{r},t) + \sigma^c_{ij}(\mathbf{r},t)$. The kinetic and collisional stresses are given by, respectively [22],

$$\sigma^k_{ij}(\mathbf{r},t) = \sum_{\alpha=1}^{N} m_\alpha u_i'^{\alpha} u_j'^{\alpha}(\mathbf{r},t)\times\Theta[\mathbf{r}-\mathbf{r}_\alpha(t)], \tag{10}$$

$$\sigma^c_{ij}(\mathbf{r},t) = -\frac{1}{2}\sum_{\alpha,\beta,\alpha\neq\beta} f_i^{\alpha\beta}(t) r_j^{\alpha\beta}(t)\int_0^1 \Theta[\mathbf{r}-\mathbf{r}_\alpha(t)+s\mathbf{r}_{\alpha\beta}(t)]ds, \tag{11}$$

where $u_i'^{\alpha}$ is the velocity fluctuation of particle α with respected to the average velocity $\bar{U}(r,t)$ of the particles in the coarse-graining volume. The vector $\mathbf{r}^{\alpha\beta} = \mathbf{r}^\alpha - \mathbf{r}^\beta$ points from the center of particle β to the center of particle α, $f^{\alpha\beta}$ is the contact force acting between particles α and β, and Θ is the coarse-graining (CG) function. In this work, we use the Heaviside function $\Theta(\mathbf{r}) = H(w-|r|)/V$ where $V = 4/3\pi r^3$ is the coarse-graining volume and w is the coarse-graining radius. The (granular) pressure P is obtained by $P = \text{Tr}(\sigma_{ii})/3$ [22].

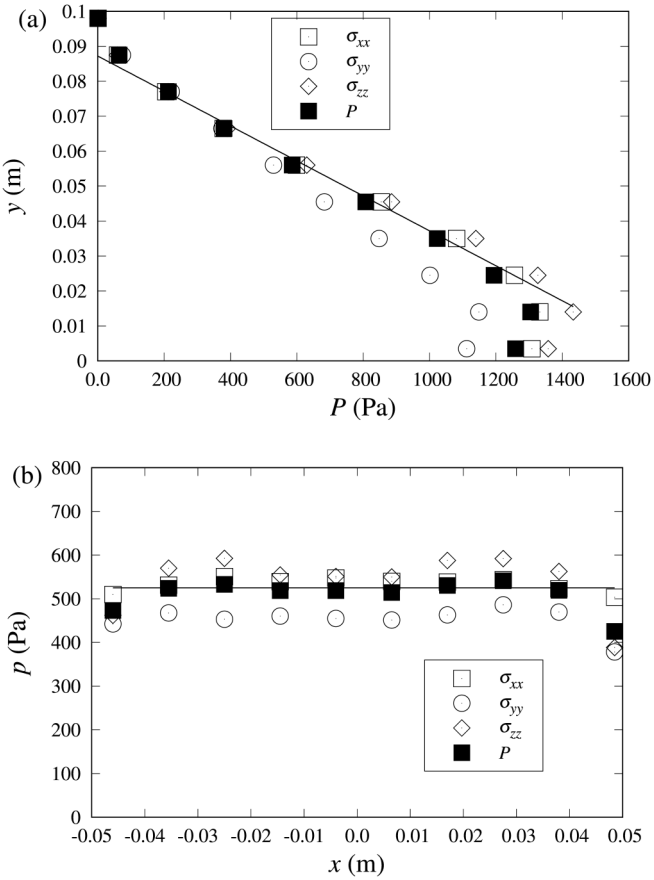

FIG. 10. (a) Granular pressure profiles in the vibrated bed along the vertical y direction. (b) Granular pressure profiles in the vibrated bed along the horizontal x direction at $y = 0.05$ m.

The obtained pressure profiles (identical system but without an intruder) along the vertical (y) and horizontal (x) directions are plotted in Figs. 10(a) and 10(b) respectively . While the pressure is almost constant along the horizontal direction, Fig. 10(b), an almost constant pressure gradient, similar to a classic hydrostatic pressure in a fluid, is established in the vertical direction, Fig. 10(a). However, at the bottom and the surface of the vibrated bed there are some appreciable deviations from a constant pressure gradient, similar to what has been observed in Ref. [45]. Since the intruder was placed at the center of the bed, these boundary effects did not affect the segregation behavior of the intruder. Using the determined pressure gradient, the buoyancy force can be calculated via

$$F_b = \int p\cdot\mathbf{n}d\tilde{\mathbf{S}} = \int\left(\frac{\partial p}{\partial x}+\frac{\partial p}{\partial y}+\frac{\partial p}{\partial z}\right)d\tilde{V} \approx \frac{\partial p}{\partial y}\tilde{V}. \tag{12}$$

Figure 11 plots a comparison between the buoyancy forces computed through the generalized Archimedean formulation, Eq. (4), and its hydrostatic definition, Eq. (12). The calculated values are very similar, suggesting that using the Voronoi volume as the effective occupied space of the intruder, the hydrostatic definition of the buoyancy force can be applied also to granular systems (using a coarse-graining derived granular pressure). However, the calculation of the buoyancy force

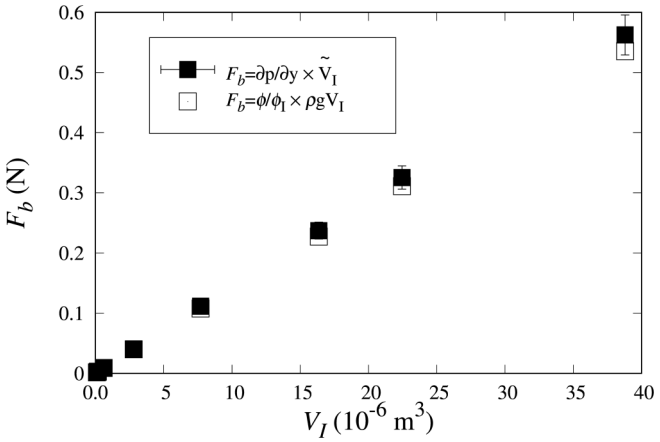

FIG. 11. Buoyancy force calculated through its hydrostatic definition, Eq. (12), and the generalized Archimedean formulation Eq. (4).

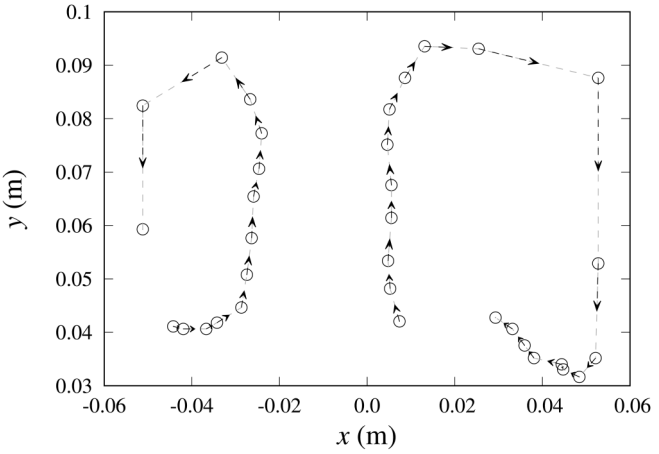

FIG. 12. Particle trajectories in the xy plane starting at $t = 150$ s for $\Gamma = 8.0$. The time interval between two successive trajectory points is equal to 2.5 s. The arrow indicates the moving direction along the time.

though its hydrodynamic definition [Eq. (12)] is rather cumbersome as it requires coarse graining, while the generalized Archimedean formulation requires only one fitting parameter (for a given system) to calculate accurately the buoyancy force acting on an intruder allowing for an effective computation for practical problems.

So far we have shown that the generalized Archimedean formulation of the buoyancy force is in very good agreement with the calculation through its hydrostatic definition, Eq. (12), or its direct numerical measurement via a virtual spring in a convection-free vibrated bed. Now we turn to a more general system in which a convective pattern is present. To formulate a force balance on the intruder an upward-directed drag force $\mathbf{F}_d$ due to an upward-directed convection (at the center of the bed) has to be considered, i.e.,

$$\mathbf{F}_{\text{lift}} = \mathbf{F}_b + \mathbf{F}_d = -(\mathbf{F}_g + \mathbf{F}_s). \tag{13}$$

The drag force is obtained by subtracting the buoyancy force from the segregation (lift) force (which is obtained through the virtual spring force Eq. (8)). If the generalized Archimedean formulation is also applicable for such convective systems, the granular drag obtained through Eq. (13) should match the values obtained through the granular drag model given by Eq. (5).

By setting the wall friction coefficient to a nonzero value, a convection pattern is established in the vibrated bed, as the cross sectional area of the bed is not exactly constant over a vibration cycle. To confirm the establishment of a convective patter, randomly selected particles are tracked in the bed. The trajectories are shown in Fig. 12 and confirm an upward motion in the center of the bed and a downward motion close to the walls. The lift force in such a convective system, as determined by Eq. (8), far exceeds the buoyancy force calculated through the generalized Archimedean formulation Eq. (4) as shown in Fig. 13. In addition, when normalized by the weight of the intruder the lift force becomes dependent on the intruder size, which distinguishes it from the weight-normalized buoyancy force in a fluid ($F_b/m_I g$) which is size independent. As the size ratio of the intruder to the bed particles increases, the weight-normalized, buoyancy force calculated by the generalized Archimedean formulation, Eq. (4), approaches $F_b/m_I g = 0.62$ whereby 0.62 is the bulk solid fraction ϕ of the bed, as expected, and $F_b/m_I g = 1$ for $d_I/d_p = 1$.

We attribute the difference between the virtual-spring derived lift force and the buoyancy force calculated via the generalized Archimedean formulation Eq. (4), to the presence of a convective pattern and hence the presence of a drag force that also acts in the vertical direction. When probing the magnitude of the relative velocity between the intruder and the bed particles, an average relative velocity of $\sim$0.2 mm/s is determined in the center of the bed, i.e., within the limits of the slow-velocity drag regime ($v \ll 0.028$ m/s). In the slow-velocity regime the drag force is independent of the relative velocity and given by Eq. (5) where β is a constant that depends on the restitution coefficient and the shape of the bed

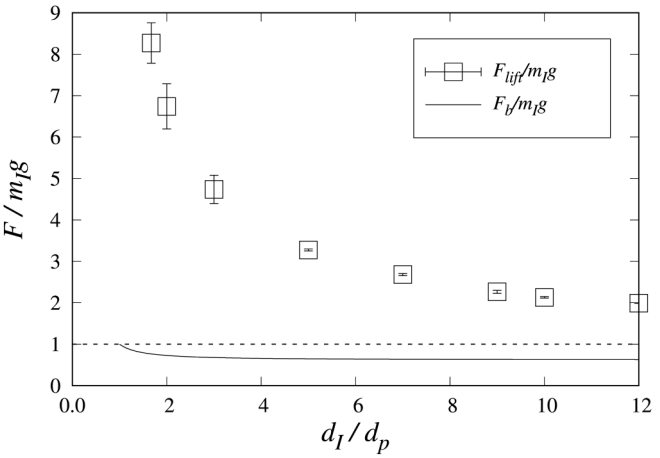

FIG. 13. (□) Numerically determined [via a virtual spring using Eq. (8)], weight-normalized lift force. The solid line is the weight-normalized buoyancy force $F_b/m_I g$ determined by the generalized Archimedean formulation, i.e., $F_b = (\phi/\phi_I)\rho_p g V_I$, where $\phi_I = (\phi - 1)S^c + 1$, with $c = -1.35$ and $\phi = 0.62$ for $\Gamma = 8.0$. The dash line is a reference line which denotes $F/m_I g = 1$.

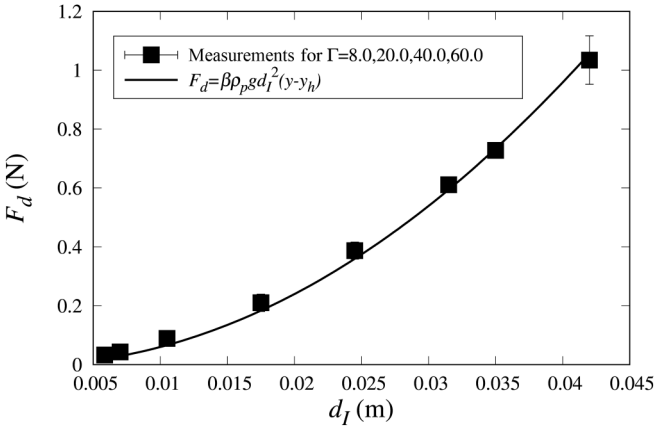

FIG. 14. (■) Drag force determined by subtracting the buoyancy force from the lift force. The lift force was measured using a virtual spring and is given by Eq. (13). The buoyancy force was calculated using the generalized Archimedean formulation, i.e., Eq. (4). The solid line gives the granular drag forces determined through $F_d = \beta\rho_p g d_I^2(y - y_h)$ with $\beta = 0.59$.

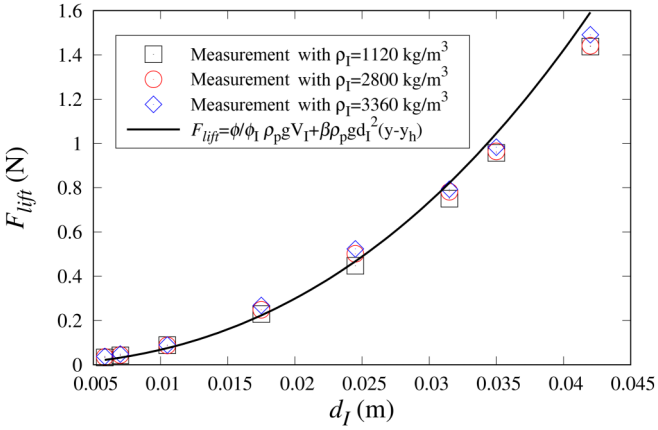

FIG. 15. Comparison of the lift force predicted by Eq. (14) and the lift force obtained numerically by a virtual spring [Eq. (8)] as a function of the intruder size for different intruder densities ρ_I.

particles [36]. Using the force balance Eq. (13), the drag force $\mathbf{F}_d$ can be obtained by subtracting the buoyancy force from the lift force. Subsequently, the granular drag force obtained through Eq. (5) can be compared to the drag force determined through Eq. (13) and in the case of a good agreement, the lift force acting on an intruder in a convective system can be expressed by

$$F_{\text{lift}} = F_b + F_d = \frac{\phi}{\phi_I}\rho_p g V_I + \beta\rho_p g(y_h - y)d_I^2. \quad (14)$$

Indeed, we observe a very good agreement between the drag forces obtained and using a least squares fitting method, β was determined as 0.59 (see Fig. 14) .

A conclusion from Eq. (14) is that the lift force acting on the intruder is independent of the intruder density, but it depends on the density of the bed particles and the intruder size. To assess the validity of these key observations, we performed additional simulations with a varying intruder density. Figure 15 confirms a good agreement between the lift force measured through the virtual spring, i.e., $F_{\text{lift}} = F_{\text{spring}} + m_I g$, and Eq. (14) using $\beta = 0.59$ (β depends on the surface properties of the particles and the shape of the intruder).

A further consequence of the formulation of the total lift force following Eq. (14) is that in a given system that falls into the slow-velocity regime, the lift force is independent of the vibration strength injected by the side wall (Γ increasing from 8 to 60 as shown in Fig. 5). This can be rationalized by the fact that for a given intruder size and position within the bed, the buoyancy force is constant as the bulk solid fraction does not vary with increasing vibration strength (Fig. 6) and the drag force depends on β which, however, is only a function of the coefficient of restitution and the intruder shape.

IV. CONCLUSION

In this study, we have verified the validity of a generalization of the Archimedean formulation of a granular buoyancy force that has been proposed originally for shear flows for vibrofluidized systems. To exclude the influence of drag forces, a convection-free system was considered, established through vibrating sidewalls and a friction coefficient of zero for particle-wall contacts. The buoyancy force calculated through the generalized Archimedean formulation, i.e., considering the Voronoi volume of the intruder, agreed very well with the values obtained from its hydrostatic definition (pressure gradient) and its direct measurement through a virtual spring. Subsequently, we have introduced an additional complexity to the system by considering also convection (through a nonzero particle-wall friction coefficient). The segregating (lift) force acting on an intruder in such a system is affected by buoyancy and drag and increases with increasing intruder size, but is independent of the vibration strength Γ (once Γ exceeds 6) and the intruder density. We demonstrate that a lift force model that combines the buoyancy force (expressed through the generalized Archimedean formulation) and a drag force (velocity-independent in the considered slow-velocity regime) predicts very accurately the value of the lift force obtained through a virtual spring. This model allowed to rationalize the independence of the segregation (lift) force on the intruder density and the vibration strength (once a critical value of $\Gamma_{cr} = 6$ is exceeded). We hope that our work can pave the way to the development of segregation models that allow us to quantitatively describe more complex systems, containing, e.g., multiple intruders and/or more complex drag force regimes.

ACKNOWLEDGMENTS

We are thankful to the Swiss National Science Foundation (Grant No. 200020_182692) and the China Scholarship Council (M.L.) for partial financial support of this work. M.L. acknowledges N.A. Conzelmann for useful comments on the latest version of this paper.

[1] J. Duran, J. Rajchenbach, and E. Clement, Phys. Rev. Lett. **70**, 2431 (1993).
[2] K. M. Hill and Y. Fan, Phys. Rev. Lett. **101**, 088001 (2008).
[3] O. Pouliquen, J. Delour, and S. B. Savage, Nature (London) **386**, 816 (1997).
[4] K. van der Vaart, P. Gajjar, G. Epely-Chauvin, N. Andreini, J. M. N. T. Gray, and C. Ancey, Phys. Rev. Lett. **114**, 238001 (2015).
[5] D. A. Huerta and J. C. Ruiz-Suarez, Phys. Rev. Lett. **93**, 069901 (2004).
[6] D. C. Hong, P. V. Quinn, and S. Luding, Phys. Rev. Lett. **86**, 3423 (2001).
[7] G. Lu and C. R. Müller, Granular Matter **22**, 50 (2020).
[8] K. A. Gillemot, E. Somfai, and T. Borzsonyi, Soft Matter **13**, 415 (2017).
[9] C. R. K. Windows-Yule, T. Weinhart, D. J. Parker, and A. R. Thornton, Phys. Rev. Lett. **112**, 098001 (2014).
[10] C. Seife, Science **309**, 82 (2005).
[11] G. Lu, J. R. Third, and C. R. Muller, Chem. Eng. Sci. **127**, 425 (2015).
[12] C. P. McLaren, T. M. Kovar, A. Penn, C. R. Muller, and C. M. Boyce, Proc. Natl. Acad. Sci. USA **116**, 9263 (2019).
[13] A. U. Vanarase, M. Alcala, J. I. J. Rozo, F. J. Muzzio, and R. J. Romanach, Chem. Eng. Sci. **65**, 5728 (2010).
[14] W. R. Ketterhagen, J. S. Curtis, C. R. Wassgren, A. Kong, P. J. Narayan, and B. C. Hancock, Chem. Eng. Sci. **62**, 6423 (2007).
[15] E. Simsek, S. Wirtz, V. Scherer, H. Kruggel-Emden, R. Grochowski, and P. Walzel, Particul. Sci. Technol. **26**, 177 (2008).
[16] E. Hamzeloo, M. Massinaei, and N. Mehrshad, Powder Technol. **261**, 185 (2014).
[17] B. Ferdowsi, C. P. Ortiz, M. Houssais, and D. J. Jerolmack, Nat. Commun. **8**, 1363 (2017).
[18] A. Rosato, K. J. Strandburg, F. Prinz, and R. H. Swendsen, Phys. Rev. Lett. **58**, 1038 (1987).
[19] J. Duran, T. Mazozi, E. Clement, and J. Rajchenbach, Phys. Rev. E **50**, 5138 (1994).
[20] R. Jullien, P. Meakin, and A. Pavlovitch, Phys. Rev. Lett. **69**, 640 (1992).
[21] R. Jullien, P. Meakin, and A. Pavlovitch, Europhys. Lett. **22**, 523 (1993).
[22] B. Andreotti, Y. Forterre, and O. Pouliquen, *Granular Media: Between Fluid and Solid* (Cambridge University Press, Cambridge, England, 2013) .
[23] J. B. Knight, H. M. Jaeger, and S. R. Nagel, Phys. Rev. Lett. **70**, 3728 (1993).
[24] W. Cooke, S. Warr, J. M. Huntley, and R. C. Ball, Phys. Rev. E **53**, 2812 (1996).
[25] D. A. Huerta and J. C. Ruiz-Suarez, Phys. Rev. Lett. **92**, 114301 (2004).
[26] T. Shinbrot and F. J. Muzzio, Phys. Rev. Lett. **81**, 4365 (1998).
[27] N. Shishodia and C. R. Wassgren, Phys. Rev. Lett. **87**, 084302 (2001).
[28] J. T. Jenkins and D. K. Yoon, Phys. Rev. Lett. **88**, 194301 (2002).
[29] V. Garzó, Phys. Rev. E **78**, 020301R (2008).
[30] F. Guillard, Y. Forterre, and O. Pouliquen, J. Fluid Mech. **807**, R1 (2016).
[31] C. S. Campbell and A. Gong, J. Fluid Mech. **164**, 107 (1986).
[32] K. M. Hill and D. S. Tan, J. Fluid Mech. **756**, 54 (2014).
[33] A. Tripathi and D. V. Khakhar, J. Fluid Mech. **717**, 643 (2013).
[34] K. van der Vaart, M. P. V. Lantman, T. Weinhart, S. Luding, C. Ancey, and A. R. Thornton, Phys. Rev. Fluids **3**, 074303 (2018).
[35] D. A. Huerta, V. Sosa, M. C. Vargas, and J. C. Ruiz-Suarez, Phys. Rev. E **72**, 031307 (2005).
[36] R. Albert, M. A. Pfeifer, A. L. Barabasi, and P. Schiffer, Phys. Rev. Lett. **82**, 205 (1999).
[37] K. Wieghardt, Annu. Rev. Fluid Mech. **7**, 89 (1975).
[38] I. Albert, J. G. Sample, A. J. Morss, S. Rajagopalan, A. L. Barabasi, and P. Schiffer, Phys. Rev. E **64**, 061303 (2001).
[39] K. A. Reddy, Y. Forterre, and O. Pouliquen, Phys. Rev. Lett. **106**, 108301 (2011).
[40] P. A. Cundall and O. D. L. Strack, Geotechnique **29**, 47 (1979).
[41] C. Kloss, C. Goniva, A. Hager, S. Amberger, and S. Pirker, Prog. Comput. Fluid Dyn. **12**, 140 (2012).
[42] C. Goldenberg, A. P. F. Atman, P. Claudin, G. Combe, and I. Goldhirsch, Phys. Rev. Lett. **96**, 168001 (2006).
[43] I. Goldhirsch, Granul. Matter **12**, 239 (2010).
[44] T. Weinhart, R. Hartkamp, A. R. Thornton, and S. Luding, Phys. Fluids **25**, 070605 (2013).
[45] T. Weinhart, A. R. Thornton, S. Luding, and O. Bokhove, Granul. Matter **14**, 289 (2012).